

Optical Radiation Measurements for Photovoltaic Applications: Instrumentation Uncertainty and Performance

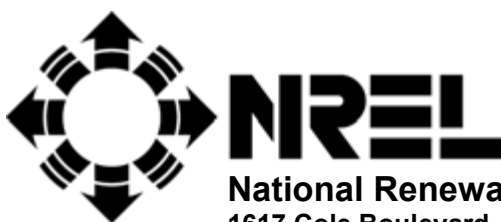
Preprint

D.R. Myers, I. Reda, S. Wilcox, and A. Andreas

*To be presented at the International Symposium
on Optical Science and Technology, SPIE's 49th
Annual Meeting
Denver, Colorado
August 2–6, 2004*

Copyright 2004 Society of Photo-Optical Instrumentation Engineers.

This paper will be published in the proceedings of the International Symposium on Optical Science and Technology, SPIE's 49th Annual Meeting on August 2-6, 2004 in Denver, Colorado; and is made available as an electronic preprint with permission of SPIE. One print or electronic copy may be made for personal use only. Systematic or multiple reproduction, distribution to multiple locations via electronic or other means, duplication of any material in this paper for a fee or for commercial purposes, or modification of the content of the paper are prohibited.



National Renewable Energy Laboratory

1617 Cole Boulevard, Golden, Colorado 80401-3393

303-275-3000 • www.nrel.gov

Operated for the U.S. Department of Energy
Office of Energy Efficiency and Renewable Energy
by Midwest Research Institute • Battelle

Contract No. DE-AC36-99-GO10337

NOTICE

The submitted manuscript has been offered by an employee of the Midwest Research Institute (MRI), a contractor of the US Government under Contract No. DE-AC36-99GO10337. Accordingly, the US Government and MRI retain a nonexclusive royalty-free license to publish or reproduce the published form of this contribution, or allow others to do so, for US Government purposes.

This report was prepared as an account of work sponsored by an agency of the United States government. Neither the United States government nor any agency thereof, nor any of their employees, makes any warranty, express or implied, or assumes any legal liability or responsibility for the accuracy, completeness, or usefulness of any information, apparatus, product, or process disclosed, or represents that its use would not infringe privately owned rights. Reference herein to any specific commercial product, process, or service by trade name, trademark, manufacturer, or otherwise does not necessarily constitute or imply its endorsement, recommendation, or favoring by the United States government or any agency thereof. The views and opinions of authors expressed herein do not necessarily state or reflect those of the United States government or any agency thereof.

Available electronically at <http://www.osti.gov/bridge>

Available for a processing fee to U.S. Department of Energy
and its contractors, in paper, from:

U.S. Department of Energy
Office of Scientific and Technical Information
P.O. Box 62
Oak Ridge, TN 37831-0062
phone: 865.576.8401
fax: 865.576.5728
email: <mailto:reports@adonis.osti.gov>

Available for sale to the public, in paper, from:

U.S. Department of Commerce
National Technical Information Service
5285 Port Royal Road
Springfield, VA 22161
phone: 800.553.6847
fax: 703.605.6900
email: orders@ntis.fedworld.gov
online ordering: <http://www.ntis.gov/ordering.htm>



Printed on paper containing at least 50% wastepaper, including 20% postconsumer waste

Optical radiation measurements for photovoltaic applications: instrumentation uncertainty and performance

Daryl R. Myers^{*a}, Ibrahim Reda^a, Stephen Wilcox^a, Afshin Andreas^a

^aNational Renewable Energy Laboratory, 1617 Cole Blvd Golden Co 80401

ABSTRACT

Evaluating the performance of photovoltaic (PV) devices in the laboratory and in the field requires accurate knowledge of the optical radiation stimulating the devices. We briefly describe the radiometric instrumentation used for characterizing broadband and spectral irradiance for PV applications. Spectral radiometric measurement systems are used to characterize solar simulators (continuous and pulsed, or flash sources) and natural sunlight. Broadband radiometers (pyranometers and pyrheliometers) are used to assess solar resources for renewable applications and develop and validate broadband solar radiation models for estimating system performance. We describe the sources and magnitudes of uncertainty associated with calibrations and measurements using these instruments. The basic calibration and measurement uncertainty associated with this instrumentation are based on the guidelines described in the International Standards Organization (ISO) and *Bureau Internationale des Poids et Mesures* (BIPM) Guide to Uncertainty in Measurement. The additional contributions to uncertainty arising from the uncertainty in characterization functions and correction schemes are discussed and illustrated. Finally, empirical comparisons of several solar radiometer instrumentation sets illustrate that the best measurement accuracy for broadband radiation is on the order of 3%, and spectrally dependent uncertainty for spectroradiometer systems range from 4% in the visible to 8% to 10% in the ultraviolet and infrared.

Keywords: Photovoltaic, performance, instrumentation, solar radiation, uncertainty

1. INTRODUCTION

Photovoltaic (PV) technologies are tested and evaluated in the laboratory and in the field using either solar simulators or natural sunlight. Figure 1 shows examples of large and small-scale solar simulators for testing prototype research and development cells, and modules. Figure 2 shows outdoor testing of flat plate PV panels, and an example of outdoor test set-up for a concentrating PV system. In each instance, a measure of the quantity and quality of optical radiation seen by the PV devices are important in establishing

technology performance^{1,2,3}. For laboratory sources, it is important that the quality of the illumination, as measured by the spectral distribution of the source, is comparable to sunlight or characterized for the departure from the spectral distribution of sunlight⁴. Spectroradiometers are used to measure the spectral distribution of simulators and natural sunlight. Outdoors, broadband radiometers are deployed as shown in figure 2a and 2b, with modules, arrays, and systems to quantify the solar input available to the test devices.



Fig. 1. Large (left) and small (right) scale solar simulators for evaluating PV performance in the laboratory.

^{*}daryl_myers@nrel.gov; phone 303-384-6768; fax 303-384-6391; <http://www.nrel.gov/rredc>

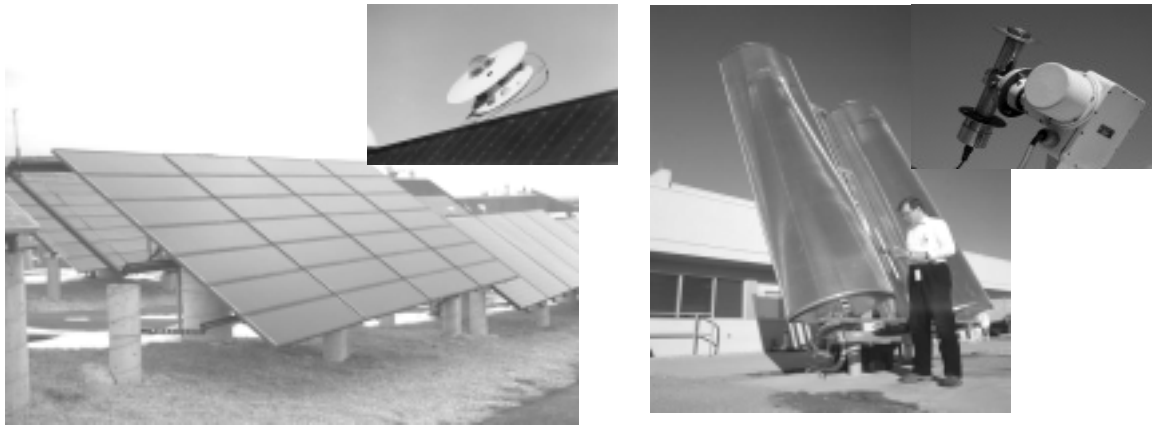


Fig. 2a (Left). Flat panel PV arrays deployed for testing outdoors at NREL. Inset shows a pyranometer measuring hemispherical solar input to arrays. Fig 2b (Right). Concentrating PV system at NREL for testing. Inset is pyrheliometer for measuring collimated direct beam solar radiation utilized by such systems.

In all cases, the calibration and measurement uncertainty of the radiometric instrumentation used is important⁵. In this paper, we discuss calibration and measurement uncertainty for each of these radiometric instruments.

2. SPECTRORADIOMETER CALIBRATION AND MEASUREMENTS

2.1 Spectral Instrumentation and calibration

Spectroradiometers used at the National Renewable Energy Laboratory (NREL) include classic scanning grating monochromator and diode array spectroradiometers⁶. Figure 3 is an example of a scanning grating monochromator system being set up to measure an illumination source in an environmental chamber. The calibration of these spectroradiometers is performed with respect to standards of spectral irradiance purchased directly from the National Institute of Standards and Technology (NIST) Optical Technology Division[†].

NIST provides a calibrated 1000 W incandescent tungsten halogen lamp with tabulated spectral irradiance data at about 30 wavelengths⁷. The lamp is calibrated at a certain direct current (DC), usually 8.2 amperes, and a specified distance (500 mm) from the front surface of the lamp bi-post pins. The user must reproduce the current specified by NIST, with stability better than 0.01%. The calibration geometry, especially the calibration distance must also be reproduced as accurately as possible. This requires stable DC power supplies and precision calibration geometry set-up fixtures. Figure 4 is an example of the calibration geometry for a diode array spectrometer, showing the lamp, NIST spectral irradiance data (inset), and a close-up of the spectral irradiance standard lamp. NIST supplies a statement of uncertainty with the spectral calibration, as shown in Table 1⁷. A typical spectral calibration consists of recording the response of the spectroradiometer system, including input optics, monochromator, and detectors, when viewing the calibration source (spectral standard lamp) at each wavelength. Figure 5 displays a typical response curve and the spectral distribution of the lamp source.



Fig 3. Scanning grating monochromator with integrating sphere input optic.

[†] see <http://physics.nist.gov/Divisions/Div844/facilities/fascal/fascal.html>

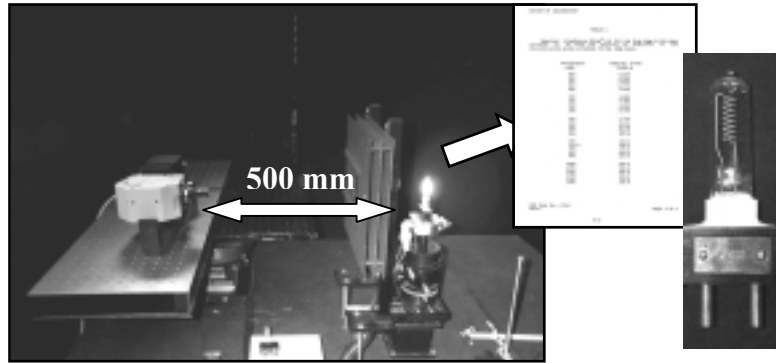


Fig.4. Example of spectral irradiance calibration configuration using NIST Standard of Spectral Irradiance (at right).

Table 1. NIST specified uncertainty in standards of spectral irradiance⁷.

Wavelength (nm)	Typical Values (W/cm ⁻²)	Relative Expanded Uncertainty in %, k=2
250	0.2	1.8
350	7.0	1.1
655	170	0.9
900	215	1.1
1600	115	1.4
2400	40	4.4

In addition to the NIST calibration uncertainty mentioned above, additional sources of uncertainty in the local laboratory calibrations, and in various measurement scenarios must be accounted for, as described in the next section.

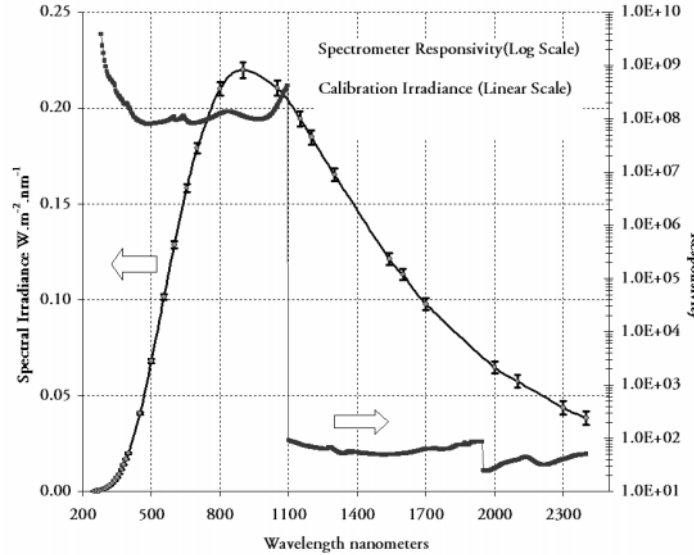


Fig. 5. NIST spectral irradiance standard lamp data and curve-fit (with NIST error bars; linear axis) and typical spectrometer response function (thick line; log axis; step at 1100 nm and 1950 nm due to detector change).

2.2 Uncertainty Analysis

Every measurement only approximates the quantity being measured, and is incomplete without a quantitative uncertainty. Every element of a measurement system contributes elements of uncertainty. Historically, uncertainty analysis treated sources of uncertainty in terms of "random" and "bias" types. Random sources of uncertainty were related to the standard deviation or variance of measured data sets. Biases were estimates of deviations from a "true value". Total uncertainty (U) was computed from: $U^2 = \Sigma (\text{Bias})^2 + \Sigma (2\text{-Random})^2$. The factor of two in the random term was necessary to "inflate" the random component to provide approximately a 95% confidence interval for the computed U . The Guide to Measurement Uncertainty (GUM) of the International Bureau of Weights and Measures is currently the accepted guide for measurement uncertainty⁸. The GUM defines Type A uncertainty values as derived from statistical methods, and Type B sources as evaluated by "other means", such as scientific judgment, experience, specifications, comparisons, or calibration data. The GUM defines the concept of a "standard uncertainty" for each uncertainty type, which is an estimate of an "equivalent" standard deviation (of a specified distribution). The GUM replaces the historical factor of 2 with a "coverage factor", k (dependent upon the known or assumed statistical distribution of uncertainties), and $U^2 = \Sigma (\text{Type B})^2 + \Sigma (k \cdot \text{Type A})^2$. For small ($n < 20$) samples from a normal distribution, k may be selected from the Student's t-distribution. U is the "Expanded Uncertainty", and k is usually in the range of 2 to 3, for confidence intervals of 95% and 99%, respectively⁹. When a result, R , is functionally dependent upon several $i=1,\dots,n$ variables, x_i , the familiar propagation of error formula $U^2 = \sum_i (\partial_{x_i} R \cdot e_{x_i})^2$ is used. U is the uncertainty in the resultant; e_{x_i} is the estimated uncertainty in variable x_i ; and $\partial_{x_i} R$ is the partial derivative of the response R with respect to variable x_i , called the sensitivity function for variable x_i .

2.3 Laboratory Spectral Calibration Uncertainty

Using the NIST calibration lamp in the laboratory, the specifications of the power supply, the geometric alignment, and accuracy of the current supplied to the lamp must be considered. For each parameter, Type A and Type B estimates of uncertainty are based on specifications, previous measurements, or educated estimates. The specifications of the spectroradiometer, such as wavelength accuracy and precision, detector noise equivalent power, stray light levels, temperature coefficients, and so on, must also be considered. Table 2 lists the uncertainties associated with operating equipment and alignment of a spectroradiometer in the laboratory for the spectral range of 250 nm to 1600 nm. The equipment consists of a power supply in constant current mode; a precision standard 0.01 ohm resistor in series with the lamp; and a 6 ½ digital multimeter measuring voltage drop, and hence the current, across the standard resistor. The voltage drop is measured with a 4-wire connection to avoid lead resistance losses. Experience has shown that a 1% current error produces a 9% irradiance error at 300nm, and a 4% irradiance error at 1000 nm. Specifications involving current have been scaled to percentage error in irradiance. An analysis similar to that in table 2 can be conducted on a wavelength-by-wavelength basis¹⁰. "Combined" uncertainties are the root-sum-square (RSS) of the Type A and Type B standard uncertainties; "expanded" uncertainty is the RSS of type A and Type B standard uncertainties with the coverage factor k applied to achieve the desired confidence interval. An asterisk indicates that an entry is a standard uncertainty (equivalent standard deviation).

Table 2. Uncertainties for 95% confidence interval, spectroradiometer calibration 250 nm -1600 nm

TYPE A (Statistical)	UNC (%)	STD UNC (%)	TYPE B	UNC (%)	STD UNC (%)
Distance (2/500 mm)	0.80	0.400	NIST Transfer	1.82	0.910
Wavelength Precision	0.01	0.005	Distance	0.8	0.400
Power Current (Irr dI/di %)*0.20	0.200		Stray Light	1e-4	0.00005
NIST Lamp Precision	1.13	0.565	Lamp Alignment	0.10	0.050
Detector Sig/Noise	1.0e-4	5.0e-5	Power Current	*0.20	0.200
Sig Detection System	1.00	0.500	Shunt Bias		
Temp Sensitivity	1.00	0.500	(-0.000002 Ω)	0.04	0.020
Observed Noise (% reading)	3.00	1.500	Wavelength	0.01	0.005
TOTAL	UNCERT(%)	STD UNCERT (%)	EFFECTIVE DEG. OF FREEDOM	>100	
Type A	3.600	1.808	COVERAGE FACTOR (k)	2	
Type B	2.001	1.015	CONFIDENCE INTERVAL	95%	
COMBINED	4.154	2.077	EXPANDED UNCERTAINTY	4.147%	

The test of the quality of an uncertainty analysis is that no measured values fall outside the expected range of uncertainty. By repeated measurements of several spectral irradiance standard lamps using a spectroradiometer system calibrated using a single lamp, we can evaluate the analysis in table 2. Figure 6 compares the measurement of seven NIST spectral irradiance standards as unknown sources, using a system calibrated using an 8th lamp¹¹. The wavelength-by-wavelength envelope for the standard uncertainties shows that the estimates in table 2 are conservative, except for the region below 400 nm, where the sensitivity and signal to noise ratio of the detectors decreases greatly. Lamp 403, which had been extensively used to test purposes after the 50 hours of specified useful life, shows serious degradation in the ultraviolet-visible part of the spectrum. The other lamps had less than 10 hours of use.

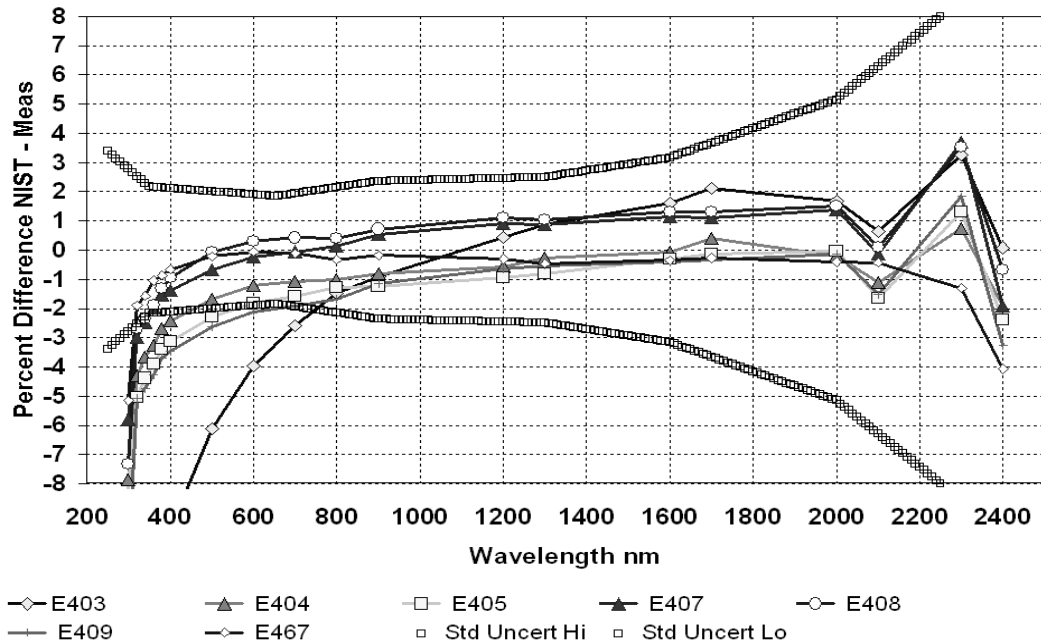


Fig. 6. Percent differences between NIST and Measured spectral irradiance at NIST data wavelengths for seven NIST spectral irradiance standard lamps (symbols on lines) measured with a spectrometer system calibrated using an 8th lamp. The envelope of estimated *standard uncertainties* is shown by the thick-hatched lines. Lamp 403 (diamond) had over 100 hours of use above the NIST specified useful lifetime of 50 operational hours.

The data in figure 6 were collected under conditions identical to calibration conditions in the metrology laboratory. When measurements are conducted under different conditions, and of significantly different spectral distributions, there will be changes in the uncertainty envelope related to differences between the calibration spectral distribution and the distribution being measured (the effect of slit scattering function)¹², stability of the spectroradiometer system, differing environmental conditions, etc. which need to be evaluated and combined with the calibration uncertainty on a case by case basis^{10,11,13}.

3. BROADBAND RADIOMETER CALIBRATIONS AND MEASUREMENTS

3.1 World Radiometric Reference and calibration techniques

As mentioned in the introduction, broadband solar radiation measurements of direct beam and hemispherical total solar radiation are important in PV module and array performance monitoring and evaluation. The basis for the calibration of these instruments is the group of seven absolute cavity radiometers (ACR), denoted as the World Standard Group (WSG - see figure 7) that defines the World Radiometric Reference (WRR), embodying the International System of Units (SI) of solar irradiance¹⁴. Romero, et al.¹⁵ showed equivalence of better than $\pm 0.05\%$ between WRR and the SI radiation scale. The WRR is transferred with an uncertainty of $\pm 0.3\%$ to national reference ACRs every five years at the World



Fig. 7. World Standard Group of absolute cavity radiometers, the mean of which establish the World Radiometric Reference), maintained at the World Meteorological Organization World Radiation Centre in Davos Switzerland.

Radiation Centre in Davos Switzerland. Pyrheliometer responsivities (R_s , output signal per stimulus unit) are derived by direct comparisons with reference ACRs traceable to WRR. Pyranometer responsivities are derived from the "component summation" technique, where a reference global irradiance (G) is derived from an absolute cavity radiometer beam measurement (B) and shaded pyranometer (diffuse) measurement (D) using $G = B \cos(z) + D$, shown symbolically in figure 8.

Responsivity (R_{sd}) of a diffuse-measuring reference pyranometer is derived in a shade-unshade calibration using $R_{sd} = (U-S)/[B^* \cos(z)]$ where U and S are the unshaded and shaded output voltages from the sensor, z is the zenith angle, and B is measured by an ACR. Procedures for this calibration are described in the American Society for Testing and Materials Standard (ASTM) E-913¹⁶. NREL developed shade-unshade pyranometer calibrations using an average responsivity at 45° zenith angle for three instrument azimuth angles to integrate over geometric response variations¹⁷. This procedure was modified to include a continuously shaded, or control pyranometer, and reducing the azimuth rotation angles to 60°. Responsivities are fit to the zenith angle, $Rs(z)$, to compute six $Rs(45^\circ)$ ¹⁸. The mean of these responsivities is used for the shaded pyranometer in the component summation calibration technique.

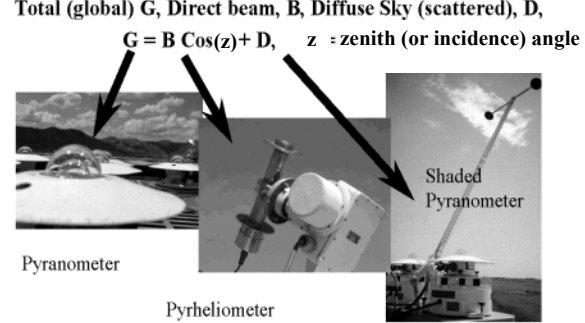


Fig.8. Solar radiation measurement instruments and the components they measure.

3.2 Radiometer uncertainty sources

Several types of detectors are used for pyrheliometer and pyranometer instruments, including silicon cells and thermal detectors such as resistance thermometers and thermopiles. Instruments based on thermopiles, behind quartz or Schott WG295 glass domes (pyranometers), or Corning 7250 glass windows (pyrheliometers) that transmit shortwave radiation from 295 nm to 2800 nm, are the most prevalent instruments and will be discussed here.

3.2.1 Thermal offsets

Studies of solar radiation instrumentation in climate research, as in the World Climate Change Research Program Baseline Surface Radiation Network (BSRN) participants¹⁹, and others^{20,21} have characterized thermal "zero offsets" in thermopile pyranometers with all-black sensors measuring diffuse radiation. The offsets produce negative engineering data at night, and clear sky diffuse irradiances lower than pure Rayleigh scattering theory predicts. The offsets occur as cold junctions of the thermopile are in a different thermal environment than the absorbing junctions. Some have proposed that shade-unshade calibrations result in "cancellation" of offsets in the shaded and unshaded state²². We believe the offsets in the two states are different, and are a source of uncertainty in shade-unshade calibrations. It is theorized that thermal infrared exchange between the sensors, domes, and (cold) sky generate these offsets. We used the MODTRAN²³ atmospheric spectral radiative transfer code to compute shortwave and longwave (infrared, 3000 nm to 10000 nm) direct beam and sky (diffuse) radiation, as in figure 9. The IR signal beyond 3000 is present in both the shaded and unshaded state of a pyranometer. However, temperature of the domes and the all black absorbing sensor is significantly lower in the shaded state. Therefore, the thermal exchange between the sky and sensor/domes *cannot* be the same. For black-and-white sensors, the reference and absorbing thermopile junctions are in a similar thermal environment (see figure 10). These radiometers have lower (~1 to 2 W/m²) offsets and produce more accurate diffuse sky measurements.

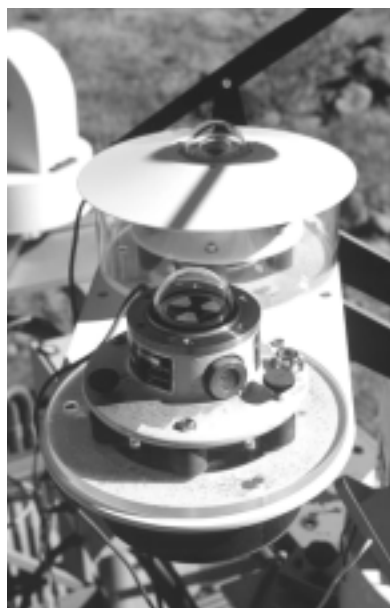


Fig. 10. All-black (top) and black-and-white sensor designs for thermopile pyranometers measuring diffuse sky radiation.

(sunshine on connectors); and electromagnetic interference (EMI)⁵. Finally, the specifications and

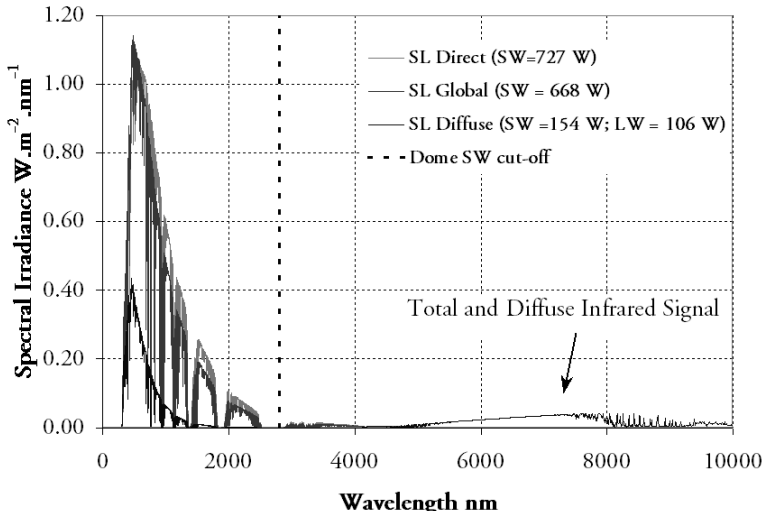


Fig. 9. MODTRAN 4.0 version 1.01 computed direct, hemispherical ("global") total, and diffuse sky spectra for sea level (SL). Zenith angle 45°, US Standard Atmosphere 1976, visibility 25 km. Top gray curve =direct beam, lowest curve=diffuse. Note infrared signal from 5000 nm to 10000nm. This signal is present when the pyranometer is shaded and unshaded, however, the temperature of the domes and the black sensor are significantly different in the two conditions.

3.2.2 Other spectral effects

There is an additional spectral affect on the shade-unshade calibration in the diffuse. The diffuse sky radiation has very little energy in the shortwave region from 1000 nm to 2800 nm, while the direct beam has significant energy in that region (see fig. 9). Therefore, nothing affecting the direct beam total irradiance between 1000 nm and 2800 nm, such as variations in atmospheric water vapor, affects the shaded pyranometer signal. Therefore, for several different water vapor concentrations, and direct normal irradiances, the same shaded signal is possible from the pyranometer. By varying total precipitable water vapor from 0.5 atm-cm to 3.5 atm-cm, MODTRAN modeling of this "spectral mismatch" effect result in differences of about 0.5% in Rs.

3.2.3 Geometric, environmental, and equipment uncertainty

Additional well-known contributors to radiometer calibration and measurement uncertainty include: accuracy of the calculation of the zenith angle; non-Lambertian cosine response of the detector surface; temperature coefficients; linearity; thermal electromotive forces (EMF); and electromagnetic interference (EMI)⁵. Finally, the specifications and

performance of the data logging equipment (resolution, precision, and accuracy) must be considered. Table 3 lists these uncertainties.

3.2.4 Sensitivity Functions

Reference diffuse radiometer responsivity calibration uncertainty, U_{shade} , computed from the propagation of error formula for the shade-unshade calibration equation is:

$$U_{\text{shade}}^2 = (\partial_U R_s \cdot e_U)^2 + (\partial_S R_s \cdot e_S)^2 + (\partial_B R_s \cdot e_B)^2 + (\partial_Z R_s \cdot e_Z)^2. \quad (1)$$

where e_U is the uncertainty in unshaded voltage, e_S uncertainty in shaded voltage, etc. Partial derivatives are sensitivity functions. For component summation, the propagation of error formula becomes:

$$U_{\text{SUM}}^2 = (\partial_U R_s \cdot e_U)^2 + (\partial_D R_s \cdot e_D)^2 + (\partial_B R_s \cdot e_B)^2 + (\partial_Z R_s \cdot e_Z)^2. \quad (2)$$

For a set of actual pyranometer voltage, beam and (black and white) diffuse data, figures 11a and 11b show sensitivity functions for each of the calibration types. Combined uncertainties depend on the product of the sensitivity functions and e_i magnitude. The largest contributions in eq. 1 are from the e_U and e_S , which *must include estimates of the thermal offset*, and data logger measurement uncertainty (typically $< 10 \mu\text{V}$). For an all-black sensor pyranometer responsivity equal to $7.0 \text{ mV per } 1000 \text{ Wm}^{-2}$, a $70 \mu\text{V}$ offset corresponds to an irradiance of -10 W/m^2 . Figures 12a and 12b compare the relative importance of increasing voltage uncertainty in U_{shade} and U_{SUM} for fixed $e_B = 4.0 \text{ Wm}^{-2}$, $e_z = 0.06^\circ$, $e_D = 2.0 \text{ Wm}^{-2}$ (black and white sensor). The component summation technique has lower total uncertainties, using only one voltage measurement.

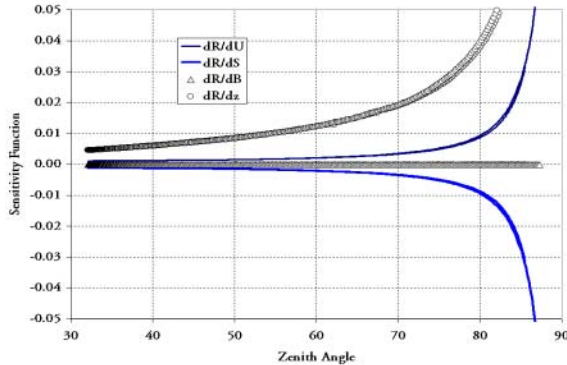


Fig. 11a. **Shade-Unshade** sensitivity functions. Shade (negative thin line) and unshade (positive thin line) voltages mirror each other. Greatest sensitivity is to zenith angle (top curve). Negligible sensitivity to beam.

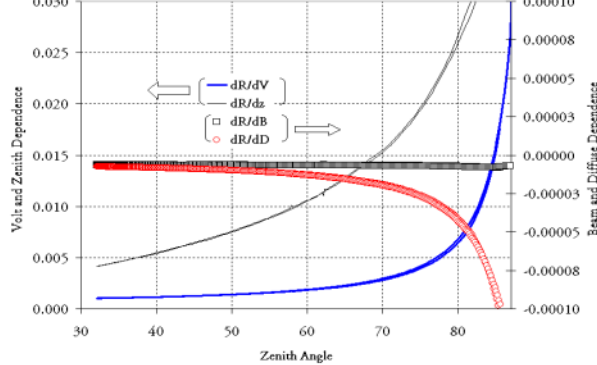


Fig. 11b. **Summation** sensitivity functions. Beam (square) and diffuse (circle) irradiances sensitivity is lower (right scale) than voltage (heavy line) and zenith angle (light line) (left scale).

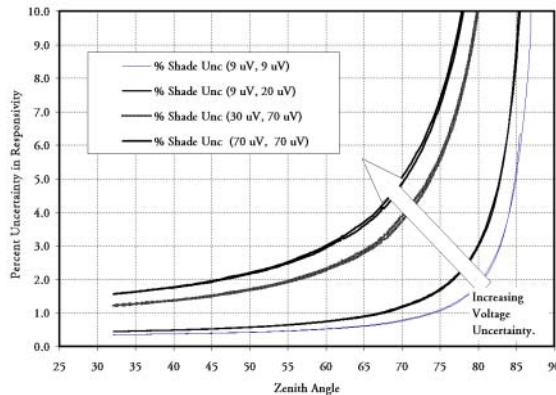


Fig. 12a. **Shade-Unshade** total uncertainty for various voltage uncertainties with fixed beam (4 Wm^{-2}) and z angle (0.06°) uncertainty. Arguments in parenthesis are uncertainty in shade unshade voltages, respectively.

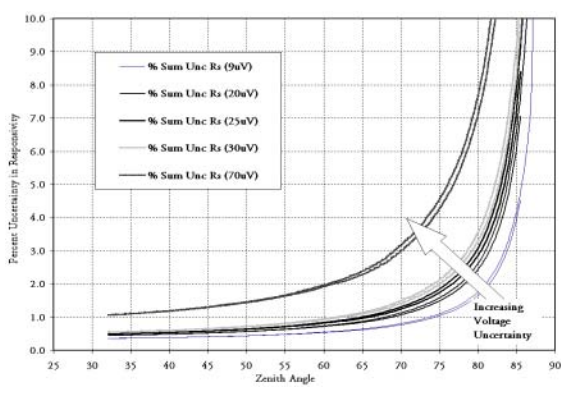


Fig. 12b. **Summation** total uncertainty for various uncertainties in test voltage measurement (parenthesis), and fixed uncertainty in beam (4 Wm^{-2}), zenith angle (0.06°), and diffuse (2 Wm^{-2}).

3.2.5 Responsivity Functions

Rather than evaluate offsets in the calibration (or measurement) process, a responsivity function derived from calibration data with the *offsets embedded in the result* should be used to retrieve the most accurate irradiance from a pyranometer²⁴. The far right curve in figure 12b assumes e_V = data logger uncertainty (9uV) only, with offset voltage zero, so the offset is built into the calibration result. Figure 13 shows the responsivity of a pyranometer (unit under test, UUT) versus zenith angle using NREL component summation calibration. The uncertainty in each pyranometer calibration responsivity point in figure 13 is summarized in table 3. The expanded uncertainty for each point in the curves of figure 5 is about 1.8%, with coverage factor $k=2$. This is the *smallest* uncertainty that can be expected of a pyranometer, under conditions identical to the calibration conditions, at a specific zenith angle.

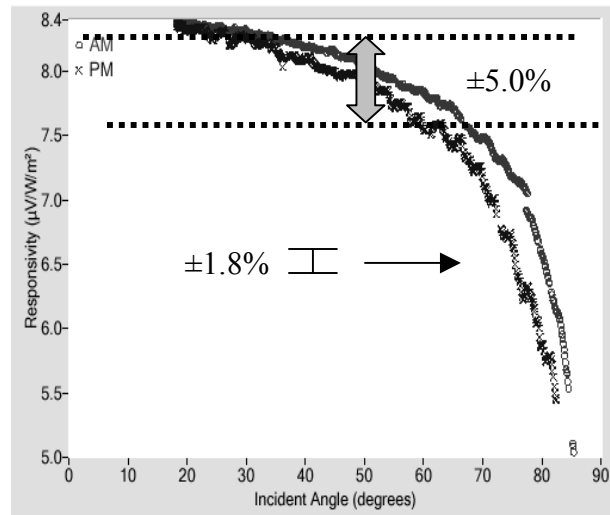


Fig. 13. Pyranometer responsivity versus solar zenith angle. Dotted lines are +5% and -5% away from mean $Rs(45^\circ)$. Uncertainty in each point is $\pm 1.8\%$.

Table 3. Uncertainties in individual Rs for summation calibration, as in Fig. 13[†]

TYPE A (Statistical)	UNC(%)	STD UNC(%)	TYPE B	UNC(%)	STD UNC(%)
WRR Transfer	*0.200	0.200	Logger Bias (9 uV/10 mv)	*0.090	0.090
Cos(z) (2° Z bin)	0.010	0.005	WRR Std U95	*0.300	0.300
Dif (2.5% D=>0.25% Ref.)	0.125	0.063	Cos(z); Z< 89 deg; 2° bin	0.010	0.005
Temperature (2° Z bin)	0.100	0.050	Temperature (2° Z bin)	0.100	0.050
Data Logger Precision	0.005	0.0025	ACR Bias (M,wind, T)	0.025	0.013
ACR (wind, T)	0.025	0.013	Temp B (event to event) 10°C	0.250	0.125
Temp Chg (10° C)	0.250	0.125	Diff Offset B&W	0.125	0.063
Diff Offset B&W	0.125	0.063	UUT IR OFFSET	*0.625	0.625
UUT IR OFFSET	0.250	0.125	Spectral Error	*0.500	0.250
EMI/Thermal EMF	0.010	0.005	EMI/Thermal EMF	0.010	0.005
TOTAL	UNCERT	STD UNCERT			
TYPE A	0.455	0.286	EFFECTIVE DEG. OF FREEDOM	>100	
TYPE B	0.910	0.872	COVERAGE FACTOR (k)	2	
COMBINED	1.017	0.918	EXPANDED UNCERTAINTY	1.84%	

[†]Cosine response is not addressed in analysis since procedure characterizes this "response"

The responsivity for a given zenith angle at the time of measurement, $Rs(m)$, can be obtained from a fit (to the response curve for calibration data in 46 2°-wide zenith angle intervals) of the form²⁴:

$$Rs(z)_{AM/PM} = \sum_{i=0}^{i=46} a_i \bullet \cos^i(z)$$

where the a_i are 46 coefficients for each morning and afternoon set of z. With this approach, uncertainty of about $\pm 1.8\%$ in measured pyranometer data can be achieved. Choosing any single responsivity, $Rs(z_0)$, the uncertainty in a measurement of global irradiance will change as the difference between $Rs(z_0)$ and $Rs(m)$ changes. The uncertainty may grow to more than 10% for zenith angles sufficiently separated. When radiometers are deployed to the field, further sources of uncertainty arise, such as differing (usually lower resolution) data logging, cleanliness, and even climatological conditions, which must be considered in addition to the calibration uncertainty computed in table 3.

3.2.6 Pyrheliometer uncertainties

As pyrheliometer signals are compared directly with the ACR signals, and there are no concerns with geometric response, or apparent thermal offsets (night-time data $\sim \pm 1.0 \text{ W m}^{-2}$), many of the contributions to total uncertainty listed in table 3 disappear. However, there are new contributions to uncertainty: the pyrheliometers have windows for continuous outdoor operation, and the ACR has no window. This may lead to spectral effects similar to those seen with respect to pyranometer domes. The ACR and pyrheliometer must be pointed at the sun, so tracking errors may arise. The final tally of the pyrheliometer uncertainty components is shown in table 4, with an expanded uncertainty for each Rs computed of 1.6%. With deployment to the field, pyrheliometer data becomes subject to additional tracking and window (cleanliness) issues, differing data logger specifications, etc. These require an additional analysis specific to the deployment for estimating a total uncertainty in the field measurement.

Table 4. Uncertainties for 95% confidence interval for individual Rs for pyrheliometer calibration.

TYPE A (Statistical)	UNC(%)	STD UNC(%)	TYPE B	UNC(%)	STD UNC(%)
WRR Transfer	*0.200	0.200	Logger Bias (9 uV/10 mv)	*0.090	0.090
Temp Response UUT	0.500	0.050	WRR Std U95	*0.300	0.300
Data Logger Precision	0.005	0.0025	Temp Response UUT	0.500	0.250
Linearity (empirical)	0.200	0.100	ACR Bias (M,wind, T)	0.025	0.013
ACR (wind, T)	0.025	0.013	Temp B (event to event) 10°	0.250	0.125
Tracking Variations		0.250	Spectral Error	*0.500	0.500
0.125			Tracking Bias	0.250	0.0125
Spectral (window)	*0.500	0.500	EMI/Thermal EMF	0.010	0.005
EMI/Thermal EMF	0.010	0.005			
TOTAL	0.802	0.615	EFFECTIVE DEG. OF FREEDOM	>100	
TYPE A	0.802	0.615	COVERAGE FACTOR (k)	2	
TYPE B	0.851	0.504	CONFIDENCE INTERVAL	95%	
COMBINED	1.169	0.918	EXPANDED UNCERTAINTY	1.59%	

CONCLUSIONS

We applied currently recommended procedures for uncertainty analysis to spectral and broadband radiometers used to evaluate the quality and quantity of optical radiation encountered during testing and performance evaluation of photovoltaic devices. Spectral calibrations and measurements have wavelength dependent envelopes of uncertainty, limited mainly by the uncertainty in the primary standards of spectral irradiance provided by NIST. The best measurement uncertainty attainable is around $\pm 2\%$ in the visible, growing to $\pm 10\%$ in the ultraviolet and infrared regions. Sensitivity functions derived from the functional form of the shade-unshade and component summation pyranometer calibration techniques show that uncertainties in signal voltages, including thermal offset voltages, affect calibration results the most. Either calibration technique can be used to map out the combined effects of geometric and thermal offset response. In both cases, the range of deviations of the responsivity from a "flat" response will produce uncertainty in measured data that is highly dependant on the responsivity chosen. The responsivity to obtain the best-measured data ($U \sim 1.8\%$) is that for the zenith angle at the time of the measurement. That responsivity can be obtained from a functional fit to calibration responsivity as a function of zenith angle. Otherwise, uncertainty on the order of 3% to 5% or more, are assured in measured global horizontal solar radiation data. While pyrheliometer calibrations do not include the thermal offset issues associated with pyranometer calibrations, they are influenced by other effects, such as tracking errors that limit the best measurements, under conditions similar to calibration conditions, to an uncertainty of $\pm 1.6\%$. In all cases, deployment of any of this instrumentation under conditions far removed from the calibration conditions will result in uncertainties in measured data that exceed, possibly greatly, the "best" uncertainties described here.

ACKNOWLEDGMENTS

This work was performed at the National Renewable Energy Laboratory under contract number DE-AC36-99GO10337 with the U.S. Department of Energy.

REFERENCES

1. Emery, K., "The rating of photovoltaic performance," *IEEE Transactions on Electron Devices*, **46**: pp. 1928-1931, 1999.
2. ASTM, "Standard test methods for electrical performance of nonconcentrator terrestrial photovoltaic modules and arrays using reference cells," Standard E1036. American Society for Testing and Materials, West Conshohocken, 1998.
3. Pearsall, N.M., K.A. Emery, M. Davies, "Influence of reference cell and spectrum on the measurement of solar cells." *7th European PV Solar Energy Conference. Sevilla, Spain*, Institute of Electrical and Electronic Engineers, Piscataway, 1996.
4. ASTM, "Standard specification for solar simulation for terrestrial photovoltaic testing," *Standard E927-97*, American Society for Testing and Materials, West Conshocken, 1997.
5. Myers, D.R., K.A. Emery, T.L. Stoffel, "Uncertainty estimates of global solar irradiance measurements used to evaluate PVdevice performance," *Solar Cells*, **27**: pp. 455-464, 1989.
6. Myers, D., "Radiometric instrumentation and measurements guide for photovoltaic performance testing," TP-560-21774, National Renewable Energy Laboratory, Golden, 1997.
7. Walker, J.H., et al., NBS Special Publication 250-20 "Spectral Irradiance Calibrations," National Institute of Standards and Technology, Gaithersburg, 1987.
8. BIPM, IEC, IFCC, ISO, IUPAC, IUPAP and OIML, "Guide to the expression of uncertainty in measurement,.." ISO TAG 4, Geneva, 1995.
9. Taylor, B.N., C.E. Kuyatt, "Guidelines for evaluation and expressing the uncertainty of NIST measurement results," NIST Technical Note 1297, National Institute of Standards and Technology, Gaithersburg, 1987.
10. Myers, D.R., "Estimates of uncertainty in measured spectra in the SERIsolar spectral radiation data base," *Solar Energy*, **43**(6): pp. 347-353. 1989.
11. Kiedron, P.W., J.J. Michalsky, J.L. Berndt, L.C. Harrison, "A comparison of spectral irradiance standards used to calibrate shortwave radiometers and spectroradiometers," *Applied Optics*, **38**: pp. 2432-2439. 1999.
12. Kostkowski, H.J., *Reliable Spectroradiometry*, Spectroradiometry Consulting, La Plata, 1997.
13. Nann, S., K. Emery, "Spectral effects on pv device rating," *Solar Energy Materials and Solar Cells*, **27**: pp. 189-216, 1992.
14. Anonymous, "International Pyrheliometer Comparison IPC-IX, 25 September - 13 October 2000: Results and Symposium," MeteoSwiss, Davos and Zurich, 2001.
15. Romero, J., N.P. Fox, C. Frohlich, "Improved comparison of the world radiometric reference and the SI radiometric scale," *Metrologia*, **32**(6): pp. 523-524, 1996.
16. ASTM, "Standard method for calibration of reference pyranometers with axis vertical by the shading method," ASTM E913-97, American Society for Testing and Materials, West Conshocken, 1997.
17. Reda, I., D. Myers, "Calculating the diffuse responsivity of solar pyranometers," NREL/TP-560-26483, National Renewable Energy Laboratory, Golden, 1999.
18. Reda, I., T. Stoffel, D. Myers, "A method to calibrate a solar pyranometer for measuring reference diffuse irradiance," *Solar Energy*, **74**: pp. 103-112, 2003.
19. Dutton, E.G., et al., "Measurement of broadband diffuse solar irradiance using current commercial instrumentation with a correction for thermal offset errors," *Journal of Atmospheric and Oceanic Technology*, **18**(3): pp. 297-314, 2001.
20. Gulbrandsen, A., "On the use of pyranometers in the study of spectral solar radiation and atmospheric aerosols," *Journal of Applied Meteorology*, **17**: pp. 899-904, 1978.
21. Haeflalin, M., et al., "Determination of the thermal offset of the Eppley precision spectral pyranometer," *Applied Optics*, **40**(4): p. 472-484, 2001.
22. Philipona, R., "Underestimation of solar global and diffuse radiation measured at the Earth's surface," *Journal of Geophysical Research*, **107**(D22): pp. ACL 15-1-ACL 15.8, 2001.

23. Berk, A., et al., "MODTRAN4 radiative transfer modeling for atmospheric correction," *SPIE Proceedings, Optical Spectroscopic Techniques and Instrumentation for Atmospheric and Space Research III*, Vol. 3756, pp. 348-353, Society for Photo-Optical Instrumentation Engineers, Bellingham, 1999.
24. Reda, I., "Improving the accuracy of using pyranometers to measure clear sky global irradiance," NREL/TP-560-24833, National Renewable Energy Laboratory, Golden, 1998.